Shock revival in core-collapse supernovae assisted by heavy axionlike particles

Kanji Mori,[1,*] Tomoya Takiwaki,[2] Kei Kotake,[1,3] and Shunsaku Horiuchi[4,5]

[1]Research Institute of Stellar Explosive Phenomena, Fukuoka University, 8-19-1 Nanakuma, Jonan-ku, Fukuoka-shi, Fukuoka 814-0180, Japan
[2]National Astronomical Observatory of Japan, 2-21-1 Osawa, Mitaka, Tokyo 181-8588, Japan
[3]Department of Applied Physics, Faculty of Science, Fukuoka University, 8-19-1 Nanakuma, Jonan-ku, Fukuoka-shi, Fukuoka 814-0180, Japan
[4]Center for Neutrino Physics, Department of Physics, Virginia Tech, Blacksburg, Virginia 24061, USA
[5]Kavli IPMU (WPI), UTIAS, The University of Tokyo, Kashiwa, Chiba 277-8583, Japan

(Received 7 December 2021; accepted 21 February 2022; published 14 March 2022)

Axionlike particles (ALPs) are a class of hypothetical pseudoscalar particles which feebly interact with ordinary matter. The hot plasma of core-collapse supernovae is a possible laboratory to explore physics beyond the standard model including ALPs. Once produced, some of the ALPs can be absorbed by the supernova matter and affect energy transfer. In this study, we calculate the ALP emission in core-collapse supernovae and the backreaction on supernova dynamics consistently. It is found that the stalled bounce shock can be revived if the coupling between ALPs and photons is as high as $g_{a\gamma} \sim 10^{-9}$ GeV^{-1} and the ALP mass is 40–400 MeV. Most of the models result in more energetic explosions than the average observed supernova. While this can be used to place constraints on those ALPs, long-term simulations across multiple progenitors need to be further investigated to place robust limits.

DOI: 10.1103/PhysRevD.105.063009

I. INTRODUCTION

Axionlike particles (ALPs) are exotic pseudoscalar particles that possibly interact with photons [e.g., [1,2]]. The ALP-photon interaction is described by the Lagrangian [3]

$$\mathcal{L} = -\frac{1}{4} g_{a\gamma} F_{\mu\nu} \tilde{F}^{\mu\nu} a, \tag{1}$$

where a is the ALP field, $F_{\mu\nu}$ is the electromagnetic tensor and $\tilde{F}_{\mu\nu}$ is its dual, and $g_{a\gamma}$ is the coupling constant between ALPs and photons. The coupling with standard model particles leads to the production of ALPs in astrophysical plasma.

Heavy ALPs with a mass of $m_a \gtrsim 1$ MeV have been explored by experiments and cosmological and astrophysical arguments. Terrestrial experiments with particle accelerators have excluded a large part of the ALP parameter space with $g_{a\gamma} \gtrsim 10^{-7}$ GeV^{-1} [4–7]. Also, standard cosmology, including big bang nucleosynthesis and the cosmic microwave background, provides strong constraints on the ALP parameters [8,9].

Astrophysical arguments often utilize stars and supernovae (SNe) as ALP factories. Since ALPs produced in stars affect the energy transfer, the parameters can be constrained by comparison between stellar models and astronomical observations. For example, additional energy losses from stars induced by ALPs shorten the lifetime of horizontal branch stars in globular clusters and affect the stellar population [10]. The energy loss also changes the structure of asymptotic giant branch stars and leads to a different initial-final mass relation of white dwarfs [11]. Many ALPs can also be produced in core-collapse SNe (CCSNe). As a result, stringent constraints can be obtained from the neutrino burst from SN 1987A [12,13] and the explosion energy [14,15]. A part of heavy ALPs can escape from astronomical objects and decay into photons during propagation in the interstellar space. Nondetection of γ rays from SN 1987A then gives another constraint on the ALP mass and $g_{a\gamma}$. These astrophysical considerations constrain the ALP-photon coupling to approximately $g_{a\gamma} \lesssim 10^{-10} - 10^{-9}$ GeV^{-1} across a broad range of ALP mass. In the future, γ rays from nearby core-collapse and thermonuclear SNe and hypernovae [16–19] may lead to additional constraints.

In previous works of CCSNe, the ALP production and the hydrodynamics were decoupled from each other. Although one can postprocess the calculation of the ALP luminosity, the backreaction on SN dynamics cannot be investigated in this way. Nevertheless, Refs. [13,20] recently pointed out that heating in the SN gain region due to heavy ALPs can reach $\sim 10^{52}$ erg s^{-1} if the ALP mass is

*kanji.mori@fukuoka-u.ac.jp

$m_a \sim 200$ MeV. In one-dimensional SN models, the shock stalls and a successful explosion cannot be obtained (see, e.g., Refs. [21,22] for reviews). However, it has been reported that beyond Standard Model particles such as radiatively decaying ALPs [23] and sterile neutrinos [24] may cause additional heating of the shock that can lead to shock revival and significantly affect the explosion mechanism. Also, since a part of the neutrino energy may be carried out by ALPs, neutrino and gravitational wave signals from a SN may be altered. It is therefore desirable to investigate the backreaction on hydrodynamics self-consistently.

In this study, we perform a series of one-dimensional hydrodynamical simulations of stellar core collapse including both ALP production and their backreactions. We show that depending on the ALP mass and its photon coupling, we can obtain shock revival due to axion energy transport in a progenitor which does not explode when ALPs are not included.

This paper is organized as follows. In Secs. II and III, the prescription for the ALP production and absorption rates is discussed, respectively. In Sec. IV, we explain the setup for our SN models and the implementation of ALP heating. In Sec. V, we show the results of our calculations. In Sec. VI, we summarize our results and discuss future prospects.

II. ALP PRODUCTION RATES

In this study, we consider photophilic ALPs that interact with photons. We take into account two processes for ALP production: the Primakoff process ($\gamma + p \to a + p$) catalyzed by protons and the photon coalescence ($\gamma + \gamma \to a$).

The Primakoff rate is given as [25]

$$\Gamma_{\gamma\to a} = g_{a\gamma}^2 \frac{T\kappa^2 p}{32\pi E}\left(\frac{((k+p)^2+\kappa^2)((k-p)^2+\kappa^2)}{4kp\kappa^2} \times \ln\left(\frac{(k+p)^2+\kappa^2}{(k-p)^2+\kappa^2}\right) - \frac{(k^2-p^2)^2}{4kp\kappa^2}\ln\left(\frac{(k+p)^2}{(k-p)^2}\right) - 1\right), \tag{2}$$

where T is the temperature, E is the ALP energy, $p = \sqrt{E^2 - m_a^2}$ is the ALP momentum, $k = \sqrt{\omega^2 - \omega_{\rm pl}^2}$ is the wave number of photons in plasma, ω is the photon energy, $\omega_{\rm pl} \approx 16.3$ MeV $Y_e^{\frac{1}{3}}(\rho/10^{14}\ {\rm g\,cm^{-3}})^{\frac{1}{3}}$ is the plasma frequency [26], Y_e is the electron mole fraction, $\kappa = \sqrt{4\pi\alpha n_p^{\rm eff}/T}$ is the Debye-Hückel scale, $\alpha \approx 1/137$ is the fine-structure constant, and $n_p^{\rm eff}$ is the effective proton number density. The energy conservation leads to $E = \omega$. The proton number density with the Pauli blocking effect is defined as

$$n_p^{\rm eff} = 2\int \frac{d^3\mathbf{p}}{(2\pi)^3} f_p(1-f_p), \tag{3}$$

where f_p is the Fermi-Dirac distribution of protons that depends on the proton chemical potential and the effective proton mass in plasma. The chemical potential is determined from the relation

$$n_p = 2\int \frac{d^3\mathbf{p}}{(2\pi)^3} f_p, \tag{4}$$

where n_p is the number density of protons. The effective proton mass is calculated as [27,28]

$$m_p^*(\rho) = \frac{m_p}{1 + \frac{a\rho}{\rho_{\rm nuc}}}, \tag{5}$$

where $m_p \approx 938$ MeV is the proton mass, $\rho_{\rm nuc} = 0.16 m_p$ fm^{-3} is the saturation density, and a is a constant that is determined by an equation $m_p^*(\rho_{\rm nuc}) = 0.8 m_p$.

The energy loss rate induced by the Primakoff process is written as

$$Q_{\rm cool} = \int_{m_a}^{\infty} dEE\frac{d^2 n_a}{dtdE} = 2\int \frac{d^3\mathbf{k}}{(2\pi)^3}\Gamma_{\gamma\to a}\omega f(\omega), \tag{6}$$

where $f(\omega)$ is the Bose-Einstein distribution of photons.

When ALPs are heavier than $2\omega_{\rm pl}$, the photon coalescence contributes to the ALP production. The photon coalescence rate is given as [25]

$$\frac{d^2 n_a}{dtdE} = g_{a\gamma}^2 \frac{m_a^4}{128\pi^3} p\left(1 - \frac{4\omega_{\rm pl}^2}{m_a^2}\right)^{\frac{3}{2}} e^{-\frac{E}{T}}. \tag{7}$$

The energy loss rate due to the photon coalescence is then

$$Q_{\rm cool} = \int_{m_a}^{\infty} dEE\frac{d^2 n_a}{dtdE}. \tag{8}$$

III. ALP ABSORPTION RATES

Once produced, ALPs propagate through the SN matter. If they are absorbed by the matter during propagation, they affect the energy transfer in the SN. In this study, we take into account the inverse Primakoff process ($a \to \gamma$) and the radiative decay ($a \to \gamma\gamma$) as ALP absorption processes [13].

The inverse Primakoff rate is written as $\Gamma_{a\to\gamma} = 2\Gamma_{\gamma\to a}/\beta_E$. The mean free path (MFP) of ALPs due to the inverse Primakoff process is given by $\lambda_{a\to\gamma} = \beta_E\gamma_E/\Gamma_{a\to\gamma}$, where γ_E is the Lorentz factor of ALPs and $\beta_E = \sqrt{1-\gamma_E^{-2}}$. The radiative decay rate is estimated as

$$\Gamma_{a\to\gamma\gamma} = g_{a\gamma}^2 \frac{m_a^3}{64\pi}\left(1-\frac{4\omega_{\rm pl}^2}{m_a^2}\right)^{\frac{3}{2}}. \quad (9)$$

The MFP from this process is given as $\lambda_{a\to\gamma\gamma} = \beta_E\gamma_E/\Gamma_{a\to\gamma\gamma}$. The total MFP is then given by $\lambda_a = (\lambda_{a\to\gamma}^{-1} + \lambda_{a\to\gamma\gamma}^{-1})^{-1}$. Although the MFP is dependent on ALP energy E, we average E over the ALP spectrum to reduce the computational cost.

IV. CORE-COLLAPSE MODELS

We incorporate the effect of ALPs in `3DnSNe` [29] and perform one-dimensional SN hydrodynamical simulations. The code adopts the HLLC solver [30] to solve the Riemann problem. The nuclear equation of state is based on Ref. [31] with incompressibility of 220 MeV. The neutrino transport is treated with a three-flavor isotropic diffusion source approximation [32–34]. The employed neutrino reactions are the same as set6abc of Ref. [34]. We adopt nonrotating progenitors [35] with the zero-age main sequence (ZAMS) masses of 20 $M_\odot$ and 11.2 $M_\odot$ and the Solar metallicity as the initial conditions. Although a thorough sensitivity study on the progenitor mass dependence is beyond the scope of this work, the two progenitors are adopted because they are typical models that would leave a neutron star as an outcome of the core collapse (e.g., Ref. [36]).

At the final stage of the evolution of massive stars, photodisintegration of iron destabilizes the stellar core and core collapse commences. When the density of the collapsed core reaches the nuclear saturation density, the core stiffens due to the nuclear repulsive force and the core bounce occurs. A shock is then formed in the core because the SN material continues to accrete from the envelope. The temperature is highest at a radius of ∼10 km because the shock there heats the accreting material. Eventually, the shock wave that is formed by the core bounce stalls because of energy losses due to the photodisintegration of heavy elements. In our model without ALPs, the stalled shock is not energetically revived, consistent with the literature where one-dimensional explosions are achieved only in lighter ∼8–10 $M_\odot$ stars [37].

In order to incorporate the effects of ALPs in SN models, we treat the ALP transport as follows. The evolution of the ALP energy per unit volume $\mathcal{E}$ is described by

$$\frac{\partial\mathcal{E}}{\partial t} + \nabla\cdot\boldsymbol{\mathcal{F}} = Q_{\rm cool} - Q_{\rm heat}, \quad (10)$$

where $\boldsymbol{\mathcal{F}}$ is the ALP energy flux and $Q_{\rm heat}$ is the heating rate per unit volume due to ALPs. If we assume stationarity and spherical symmetry, the equation simplifies to

$$\frac{1}{4\pi r^2}\frac{\partial}{\partial r}(L) = Q_{\rm cool} - Q_{\rm heat}, \quad (11)$$

where $L = 4\pi r^2\mathcal{F}$. Equation (11) is discretized in radius as

$$L_{i+\frac{1}{2}} = L_{i-\frac{1}{2}} + (Q_{{\rm cool},i} - Q_{{\rm heat},i})\Delta V_i, \quad (12)$$

for the ith cell. Here $L_{i+\frac{1}{2}}$ and $L_{i-\frac{1}{2}}$ are the ALP luminosities at the cell edges, and ΔV_i is the cell volume. The heating rate $Q_{\rm heat}$ is evaluated as

$$Q_{{\rm heat},i}\Delta V_i = L_{i-\frac{1}{2}}\left(1-\exp\left(-\frac{r_{i+1}-r_i}{\lambda_{a,i}}\right)\right). \quad (13)$$

The nth step of the internal energy of the matter, $e_{\rm int}^n$, is then updated as

$$e_{{\rm int},i}^{n+1} = e_{{\rm int},i}^n + (Q_{{\rm heat},i}^n - Q_{{\rm cool},i}^n)\Delta t, \quad (14)$$

where Δt is the time step.

Similarly, the number $L_{\rm n}$ of ALPs that pass a mass shell per unit time follows the relation

$$L_{{\rm n},i+\frac{1}{2}} = L_{{\rm n},i-\frac{1}{2}} + (\dot{N}_{{\rm cool},i} - \dot{N}_{{\rm heat},i})\Delta V_i, \quad (15)$$

where $\dot{N}_{{\rm cool},i}$ ($\dot{N}_{{\rm heat},i}$) is the number of ALPs produced (absorbed) in the ith cell per unit time. The number of absorbed ALPs is estimated by

$$\dot{N}_{{\rm heat},i}\Delta V_i = L_{{\rm n},i-\frac{1}{2}}\left(1-\exp\left(-\frac{r_{i+1}-r_i}{\lambda_{a,i}}\right)\right). \quad (16)$$

The average ALP energy $E_{{\rm ave},i}$ in the ith cell is then estimated as $E_{{\rm ave},i} = L_{i-\frac{1}{2}}/L_{{\rm n},i-\frac{1}{2}}$. The averaged energy is used to calculate the MFP of ALPs.

V. RESULTS

We perform two core-collapse simulations without ALPs and 24 SN simulations with $m_a = 50$–800 MeV and $g_{10} = g_{a\gamma}/(10^{-10}\ {\rm GeV}^{-1}) = 4$–$40$. Our focus on this range is motivated by studies employing the postprocessing method to estimate the ALP effects, and we find that the energy deposited by ALPs behind the shock can be very high [13]. The SN models developed in this study are listed in Table I. The parameter region explored by these models has not been excluded by previous works on the SN 1987A limits [13,17].

In the neutrino-driven explosion scenario, neutrinos heat up the matter behind the shock wave and help the explosion. Since most one-dimensional SN models fail to explode, it is usually argued that multidimensional effects including convection and the standing accretion shock instability are essential to achieve successful explosions (e.g., Refs. [38–42]). This argument is supported by recent multidimensional simulations, some of which reproduce 10^{51} erg explosions (e.g., Refs. [43–46]). However,

TABLE I. SN models developed in this study. Here M is the progenitor ZAMS mass, and $t_{\rm pb,400}$ is the time since the shock bounce at the moment when the shock wave reaches $r = 400$ km. The values of the explosion energy $E_{\rm exp}$ and the proto-neutron star mass $M_{\rm PNS}$ are those at $t_{\rm pb} = t_{\rm pb,400}$. The columns for the ALP cooling power L_a and the heating power $L_{\rm heat}$ show their values at $t_{\rm pb} = 200$ ms. The row with $g_{10} = 0$ represents the model without ALPs.

$M/M_\odot$	m_a [MeV]	g_{10}	Shock revival?	$t_{\rm pb,400}$ [ms]	$E_{\rm exp}$ [10^{51} erg]	$M_{\rm PNS}/M_\odot$	L_a [erg s^{-1}]	$L_{\rm heat}$ [erg s^{-1}]
20	–	0	No				0	0
20	50	4	No				3.94×10^{50}	3.88×10^{47}
20	50	10	No				2.47×10^{51}	1.50×10^{49}
20	50	20	No				9.90×10^{51}	2.38×10^{50}
20	50	40	Yes	557	0.95	1.88	3.99×10^{52}	3.70×10^{51}
20	100	4	No				1.28×10^{51}	1.58×10^{49}
20	100	10	No				7.98×10^{51}	6.00×10^{50}
20	100	20	Yes	352	1.23	1.85	3.18×10^{52}	8.50×10^{51}
20	100	40	Yes	166	2.11	1.69	1.05×10^{53}	7.55×10^{52}
20	200	4	No				3.28×10^{51}	4.75×10^{50}
20	200	10	Yes	308	1.41	1.83	2.02×10^{52}	1.26×10^{52}
20	200	20	Yes	176	0.93	1.71	6.52×10^{52}	6.37×10^{52}
20	200	40	Yes	134	0.99	1.63	1.74×10^{53}	1.73×10^{53}
20	400	4	Yes	526	0.40	1.90	1.32×10^{51}	1.08×10^{51}
20	400	10	Yes	286	0.41	1.82	8.12×10^{51}	7.95×10^{51}
20	400	20	Yes	252	0.88	1.78	3.10×10^{52}	3.03×10^{52}
20	400	40	Yes	271	1.11	1.79	1.09×10^{53}	1.05×10^{53}
20	800	4	No				8.48×10^{48}	8.48×10^{48}
20	800	10	No				5.30×10^{49}	5.30×10^{49}
20	800	20	No				2.12×10^{50}	2.12×10^{50}
20	800	40	No				8.48×10^{50}	8.48×10^{50}
11.2	–	0	No				0	0
11.2	100	4	No				3.38×10^{50}	4.70×10^{48}
11.2	100	10	No				2.10×10^{51}	1.76×10^{50}
11.2	100	20	Yes	358	0.24	1.35	8.08×10^{51}	2.39×10^{51}
11.2	100	40	Yes	122	0.22	1.30	2.30×10^{52}	1.77×10^{52}

ALPs can heat the matter as well and potentially lead to shock revival even in one-dimensional models.

A. 20 $M_\odot$ models

In this study, we adopt the 20 $M_\odot$ models as a fiducial case. Figure 1 shows the time evolution of the shock wave after the core bounce in models with $m_a = 100$ MeV. We employ coupling constants $g_{10} = 0$, 4, 10, 20, and 40, where the model with $g_{10} = 0$ is the standard model without ALPs. In the cases of $g_{10} = 0$, 4, and 10, the shock wave never exceeds $r \sim 150$ km. This stalling is similar to conventional one-dimensional models. However, the shock wave is revived in the cases of $g_{10} = 20$ and 40 because $Q_{\rm heat}$ due to ALPs is large enough in these models. This provides a new scenario to reproduce successful SN explosions even in spherically symmetric cases.

In Fig. 2, we show the ALP cooling rate $Q_{\rm cool}$ and the heating rate $Q_{\rm heat}$ as a function of radius. The time since the core bounce is fixed to $t_{\rm pb} = 200$ ms, and the ALP mass is fixed to $m_a = 100$ MeV. It is seen that the ALP production is localized at $r \sim 10$ km. This is because the temperature is the highest in this region and the ALP production rate is a steep function of T. The values of $Q_{\rm cool}$ increase as a function of g_{10} because the ALP production rates shown in

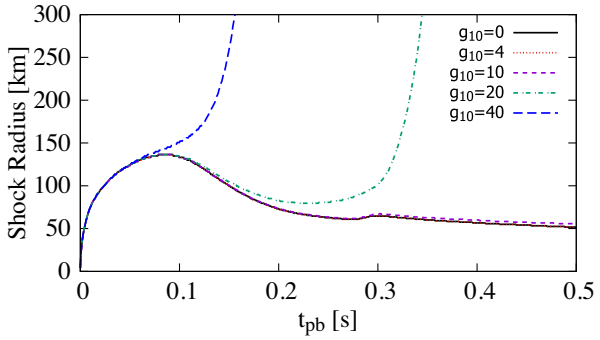

FIG. 1. Radius of the shock wave in the 20 $M_\odot$ model as a function of time $t_{\rm pb}$ since the core bounce. Shown are models including ALPs with $m_a = 100$ MeV and different couplings, as labeled, as well as the model without ALPs (black solid) for comparison.

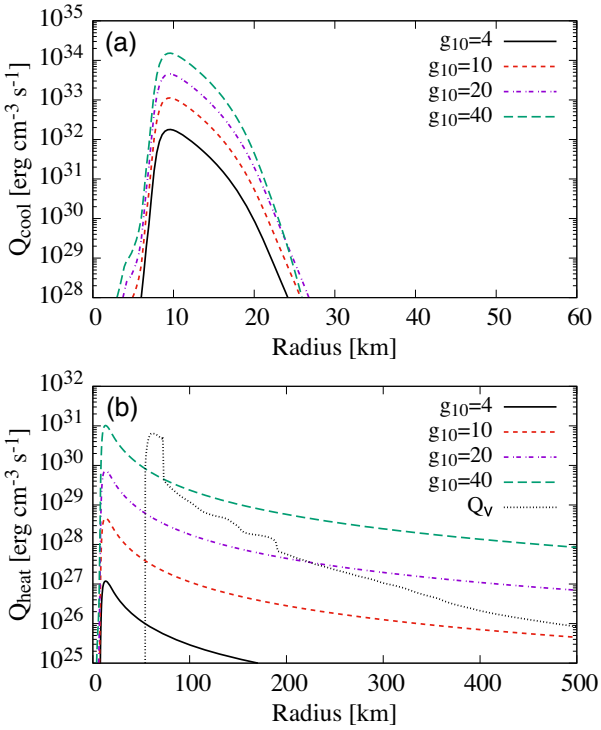

FIG. 2. Radial profiles of (a) ALP cooling rate $Q_{\rm cool}$ and (b) ALP heating rate $Q_{\rm heat}$, both in the 20 $M_\odot$ model at $t_{\rm pb} = 200$ ms. The ALP mass is fixed to $m_a = 100$ MeV. In the bottom panel, the black dotted line shows the net neutrino energy $Q_\nu = Q^\nu_{\rm heat} - Q^\nu_{\rm cool}$ in the $g_{10} = 0$ model.

Eqs. (2) and (7) are proportional to g_{10}^2. In the models with $m_a \geq 100$ MeV, the contribution of the photon coalescence is larger than that of the Primakoff process, while the contribution of the Primakoff process is dominant when $m_a = 50$ MeV.

Once produced at $r \sim 10$ km, ALPs propagate through the SN matter. A part of the ALPs is absorbed and heats up the fluid. Figure 2(b) shows the ALP heating rate for the $m_a = 100$ MeV models at $t_{\rm pb} = 200$ ms. The heating rate is the largest at $r \sim 15$ km and decreases in outer regions. The value of $Q_{\rm heat}$ is approximately proportional to g_{10}^4 because the number of produced ALPs is proportional to g_{10}^2, and the radiative decay rate is also proportional to g_{10}^2 as we see from Eq. (9). Table I shows the ALP heating power

$$L_{\rm heat} = 4\pi \int_{0\ {\rm km}}^{5000\ {\rm km}} Q_{\rm heat} r^2 dr \tag{17}$$

at $t_{\rm pb} = 200$ ms. The integration is performed over the range of the simulation, i.e., $r \in [0\ {\rm km}, 5000\ {\rm km}]$. Since the simulation is only for the SN core, $L_{\rm heat}$ in Table I does not include the deposited energy in the stellar envelope. When $m_a = 50$ MeV, $L_{\rm heat}$ is approximately proportional to g_{10}^4. The dependence of $L_{\rm heat}$ on g_{10} becomes weaker for heavier ALPs. When ALPs are as heavy as 800 MeV, one can see that $L_{\rm heat} \propto g_{10}^2$. This is because the MFP is so short that ALPs are completely trapped by the star, and hence $L_{\rm heat} \approx L_a$, where L_a is the ALP luminosity defined in Eq. (A3).

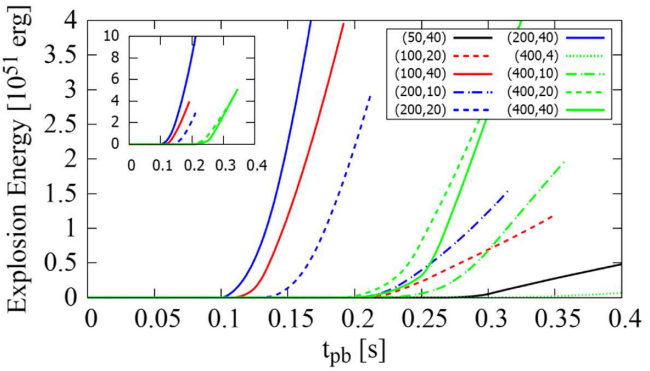

FIG. 3. Explosion energies of all 20 $M_\odot$ models that achieve successful explosions as a function of time $t_{\rm pb}$ since the core bounce. Each model is designated by a pair of $(m_a/1\ {\rm MeV}, g_{10})$. The inset panel shows the explosion energies of energetic models that exceed $E_{\rm exp} > 4 \times 10^{51}$ erg.

Figure 3 shows the explosion energy [47]

$$E_{\rm exp} = \int_D dV \left(\frac{1}{2}\rho v^2 + e - \rho\Phi \right) \tag{18}$$

for the models with successful explosions. Here v is the velocity, e is the internal energy, and Φ is the gravitational potential. The region D is the domain where the integrand is positive. In the figure, each model is designated by a pair of $(m_a/1\ {\rm MeV}, g_{10})$. In all models except for the ones with $m_a = 400$ MeV, the explosions start earlier when g_{10} is larger because of higher values of $Q_{\rm heat}$. In the model of $m_a = 400$ MeV and $g_{10} = 40$, the MFP of ALPs is as short as ~23 km. In this case, the MFP is so short that the shock wave is not heated effectively, and consequently, the monotonous dependence on g_{10} is not observed for $m_a = 400$ MeV.

The simulations are stopped before $E_{\rm exp}$ saturates. Even so, $E_{\rm exp}$ of the model with $(m_a/1\ {\rm MeV}, g_{10}) = (200, 40)$ already exceeds 10^{52} erg. Also, $E_{\rm exp}$ of the models with $(m_a/1\ {\rm MeV}, g_{10}) = (100, 40)$, (200, 20), (400, 40), and (400, 20) would eventually exceed 10^{52} erg. Given these high explosion energies, these models might be observed as broad-line type Ic SNe, whose mechanism is still under debate. Other models with $E_{\rm exp} \sim 10^{51}$ erg would be candidates for ordinary SN explosions.

Figure 4 shows $E_{\rm exp}$ at the moment when the shock wave reaches $r = 400$ km. Here, crosses represent models with failed explosion; i.e., the SN shock is not energetically revived. The explosion energies tend to increase as a function of g_{10} because higher values of $Q_{\rm heat}$ are obtained.

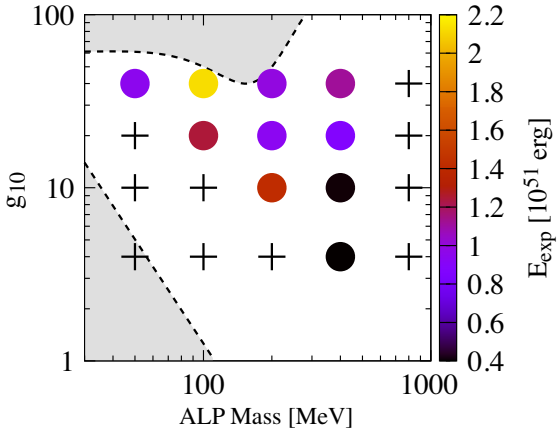

FIG. 4. Outcome of core collapse of the 20 $M_\odot$ star for various combinations of ALP parameters adopted in this work. The crosses represent models which fail to explode while filled circles represent models which successfully explode. The color shows the explosion energy in units of 10^{51} erg at the moment when the shock wave reaches $r = 400$ km. The gray regions show the SN 1987A limits [13,17].

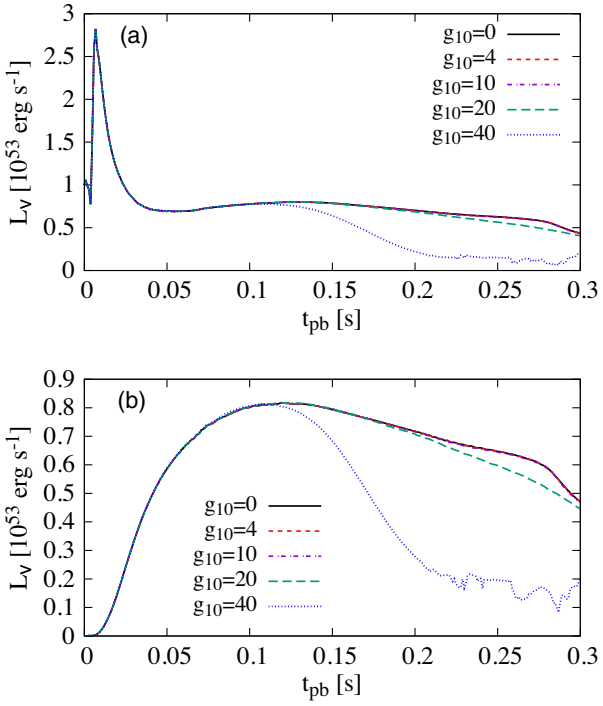

FIG. 5. Neutrino luminosities in the 20 $M_\odot$ models with $m_a = 100$ MeV. Panel (a) is for electron neutrinos, and (b) is for electron antineutrinos.

In general, heavier ALPs are conducive to explosions. This is intuitively explained by the fact that the MFP of heavier ALPs is shorter, and hence the shock wave is heated more efficiently. This trend breaks down at $m_a = 800$ MeV because the temperature in the proto-neutron star is not high enough to produce such heavy ALPs.

The ALP heating affects the proto-neutron star mass $M_{\rm PNS}$ as well. In the standard one-dimensional model, the shock revival does not occur, and the mass accretion on the proto-neutron star does not stop. As a result, the star implodes to leave a black hole. On the other hand, Table I shows the values of $M_{\rm PNS}$ in each model with successful explosion at the moment when the shock wave reaches $r = 400$ km. The remnant mass becomes smaller with the effect of ALPs because additional heating prevents the mass accretion. In our parameter region, the models show $M_{\rm PNS} \sim (1.6\text{–}1.9)M_\odot$, which is below the maximum mass of neutron stars. Hence these models will leave a neutron star as a remnant.

Figure 5 shows the ν_e and $\bar{\nu}_e$ luminosities L_ν for the models with $m_a = 100$ MeV. Electron neutrinos are mainly produced by the electron capture of protons. As a consequence, the neutronization burst is observed when the shock wave reaches the neutrino sphere. On the other hand, the $\bar{\nu}_e$ luminosity starts increasing after the ν_e luminosity because electron antineutrinos are produced by other processes such as the positron capture of neutrons, nucleon bremsstrahlung, and electron-positron annihilation. If $g_{10} \lesssim 10$, the neutrino luminosities are not affected by ALPs, while the luminosities are smaller than the standard model without ALPs if g_{10} is larger. This is because the accretion on the proto-neutron star stops in the models with successful explosions.

B. Dependence on the progenitor models

As shown in Table I, we developed five models with the 11.2 $M_\odot$ progenitor for $m_a = 100$ MeV. It is found that ALP heating can assist the shock revival as well when g_{10} is sufficiently high. Compared with the corresponding 20 $M_\odot$ models, the explosion energy in the 11.2 $M_\odot$ models is lower. This is because the peak temperature in the proto-neutron star is 51.4 MeV in the 20 $M_\odot$ models, while its value in the 11.2 $M_\odot$ models is as low as 35.4 MeV. As a result, the heating power $L_{\rm heat}$ in the lighter models is ∼3–5 times lower than that in the heavier models. Also, the mass of the proto-neutron star becomes smaller because of ALPs. It is hence expected that the mass distribution of neutron stars can be affected by ALPs, although it is beyond the scope of this study to perform a thorough investigation on stellar mass dependence.

VI. DISCUSSION AND CONCLUSIONS

In this study, we performed consistent SN simulations coupled with the production and absorption of heavy ALPs. We showed that if the mass of ALPs is 50–400 MeV and the ALP-photon coupling constant g_{10} is sufficiently high, the shock wave is efficiently heated and successful explosions are obtained. In a recent study [13], it was pointed out that the ALP luminosity from the neutrino sphere can be powerful, but using the postprocessing technique.

Our study serves as a numerical confirmation of this and supports the potential triggering of explosions.

Some of our ALP parameters resulted in energetic explosions reaching $E_{\rm exp} \sim 10^{52}$ erg. Such models are reaching the explosion energetics of broad-line type Ic SNe. Assuming the universality of ALP parameters, this would predict that most SNe would be as energetic as $\sim 10^{52}$ erg. Since it is observationally estimated that broad-line type Ic SNe represent only ∼2% of all CCSNe in giant galaxies and ∼13% in dwarf galaxies [48], such ALP parameter regions should be regarded as excluded on the basis of the explosion energy of the typical SNe [14]. On the other hand, the models with $(m_a, g_{10}) = (400\ \text{MeV}, 4)$ and (50 MeV, 40) interestingly show a moderate explosion which is similar to the majority of SNe. Future work is needed to understand the population statistics, including dependence on progenitors and nuclear equations of state, to clarify observational consequences of ALP heating and setting limits on ALP parameters.

Recently, Ref. [15] appeared online. This paper argues that the ALP parameters which lead to $E_{\rm exp} > 10^{50}$ erg should be excluded on the basis of observed low-energy SNe, although their calculation adopted postprocessing. If we adopt their criterion, all of our models with successful explosions are excluded because they show $E_{\rm exp} > 10^{50}$ erg. The excluded region for $m_a \sim 400$ MeV based on our simulations seems to be slightly broader than the result in Ref. [15]. This difference may be attributed to the difference in progenitors and microphysics such as equations of state. Also, Ref. [15] implies that our models with $m_a \leq 200$ MeV that fail to revive the shock wave are excluded as well. This argument cannot be confirmed by our simulations because the simulated region is $r < 5000$ km.

There are many potential consequences of the ALP explosion scenario, some of which we briefly discuss here. For example, ALPs may affect SN r-process nucleosynthesis. Although CCSNe used to be a candidate of the r-process site (e.g., Ref. [49]), the r-process is suppressed in recent standard models [50,51] because the irradiation by neutrinos creates a neutron-poor composition. Nevertheless, if the additional ALP heating causes an earlier shock revival, the neutrino irradiation may be reduced and the outflow may maintain a neutron-rich composition, providing helpful conditions for r-process nucleosynthesis. Recently, the effect of the hadron-quark phase transition on SN explosion has been investigated [52–54]. Contrary to the standard scenario, the r-process can occur in such models [55]. Since the dynamics of our model with ALPs is similar to these models, SN explosions induced by ALP heating might work as an r-process site. As another consequence, ALPs may affect the remnant of the stellar core collapse. Because ALPs can help shock revival, accretion on a proto-neutron star may be suppressed, compared with the standard models without ALPs. As a result, a neutron star can remain in a SN remnant instead of a black hole. This might affect the mass functions of neutron stars and black holes. It is desirable to perform systematic calculations with ALPs for a wide range of progenitors to understand the effect on remnants.

The ALP emission also influences the neutrino emission, and extreme effects can rule out ALP parameter space. Reference [13] argued that the ALP luminosity at $t_{\rm pb} = 1$ s should not exceed the neutrino luminosity $\sim 3 \times 10^{52}$ erg s^{-1} from SN 1987A and constrained the ALP parameters. Since our calculations focus on explosion dynamics at $t_{\rm pb} \lesssim 0.5$ s, our results do not contradict their argument. However, it is desirable to perform long-time simulations coupled with ALPs to verify their constraints because they have neglected the backreaction of additional cooling and heating. Similarly, ALPs may affect gravitational wave signals as well. Hence, predictions of multimessenger signals could provide unique connections with observables of future nearby SNe. While beyond the scope of this study, multidimensional simulations coupled with ALPs are indispensable to predict detailed neutrino and gravitational wave signals.

Besides astrophysical arguments, cosmology also provides probes of ALPs (e.g., Refs. [8,9,56]). ALPs could be produced in the early Universe when electrons and neutrinos are coupled. If ALPs decay after decoupling with electrons and neutrinos, neutrinos would have smaller energies than in the standard cosmological model and the number of effective neutrinos. Also, ALPs would inject photons which may dilute the neutrino and baryon densities in the epoch of big bang nucleosynthesis and affect primordial elemental abundances. Although a part of the ALP parameter space focused on in this study is excluded by cosmological arguments, some of the parameter space remains. Also, as described in Ref. [13], cosmological constraints come with additional assumptions about the cosmological model. For example, a conservative assumption about the reheating temperature may render cosmological constraints weaker by orders of magnitude [13]. Thus, it is worthwhile to explore the parameter space with independent methods to exclude the effects of systematic uncertainties.

In our simulations, we focused on ALPs that couple only with photons. However, ALPs can couple with other standard model particles such as nucleons (e.g., Refs. [57–61]) and electrons [62,63]. It has been reported that CCSNe provide information on these couplings as well, although their backreaction on hydrodynamics in the context of multidimensional simulations has not been explored in detail. It would be desirable to develop SN models to explore how additional couplings impact the energy transport in SNe. For example, since ALP-nucleon coupling can produce significantly more ALP luminosity than ALP-photon coupling (e.g., Ref. [64]), this combination could be more potent than ALP-photon coupling alone.

In summary, we numerically explored the generation and absorption of heavy ALPs self-consistently in the collapse of massive stars. We showed that ALPs can be produced in large quantities and can trigger powerful explosions. However, more studies, covering both time and progenitor diversity, are needed to fully explore the viability of the heavy ALP scenario. Nevertheless, our study supports the intriguing possibility of ALP triggered explosions. Future systematic studies may make connections with SN observables while at the same time allowing us to place constraints on ALPs.

ACKNOWLEDGMENTS

This work is supported by Research Institute of Stellar Explosive Phenomena at Fukuoka University and JSPS KAKENHI Grants No. JP21K20369, No. JP17H06364, No. JP18H01212, and No. JP21H01088. Numerical computations were carried out on the PC cluster at Center for Computational Astrophysics, National Astronomical Observatory of Japan. The work of S. H. is supported by the U.S. Department of Energy under Award No. DE-SC0020262 and NSF Grants No. AST-1908960 and No. PHY-1914409. This work was supported by World Premier International Research Center Initiative (WPI Initiative), MEXT, Japan.

APPENDIX: COMPARISON OF METHODS TO CALCULATE THE HEATING RATE

In this study, we calculated the ALP heating rate $Q_{\rm heat}$ on the basis of a recurrence relation [Eq. (12)] between successive cells. However, Ref. [13] adopted another method to calculate $Q_{\rm heat}$. In this Appendix, we compare results of the two methods.

Reference [13] defined the ALP optical depth $\tau_a(r, R)$ between radii R and r as

$$\tau_a(r,R) = \int_r^R \frac{d\tilde{r}}{\lambda_a(\langle E_a\rangle, \tilde{r})}, \tag{A1}$$

where $\lambda_a(\langle E_a\rangle, \tilde{r})$ is the MFP of ALPs at $\tilde{r}$ with the averaged ALP energy $\langle E_a\rangle$. Using τ_a, the energy deposited by ALPs at R per unit time is written as

$$L_{\rm dep}(t,R) = L_a(t)(1-\exp(-\tau_a(R_p,R))). \tag{A2}$$

Here $L_a(t)$ is the ALP luminosity defined as

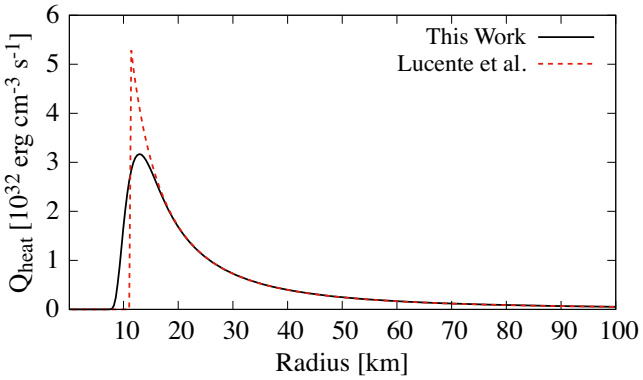

FIG. 6. ALP heating rate $Q_{\rm heat}$ at $t_{\rm pb} = 200$ ms as a function of the radius. The solid line adopts Eq. (13), and the broken line adopts Eq. (A5). The ALP mass is fixed to $m_a = 200$ MeV, and the ALP-photon coupling is fixed to $g_{10} = 40$. The SN model does not include the effect of ALPs, and the calculation of $Q_{\rm heat}$ is performed as postprocessing.

$$L_a(t) = 4\pi \int Q_{\rm cool} r^2 dr \tag{A3}$$

and R_p is the mean radius of the ALP production that is calculated as

$$R_p = \frac{\int r Q_{\rm cool} dr}{\int Q_{\rm cool} dr}. \tag{A4}$$

Since

$$L_{\rm dep}(t,R) \approx 4\pi R^2 (\Delta R) Q_{\rm heat}, \tag{A5}$$

we can calculate the ALP heating rate $Q_{\rm heat}$ from the energy deposition rate defined in Eq. (A2).

Figure 6 shows the comparison of the ALP heating rates $Q_{\rm heat}$ calculated with Eqs. (13) and (A5). Here the ALP mass is fixed to $m_a = 200$ MeV and the ALP-photon coupling is fixed to $g_{10} = 40$. In this calculation, we adopt the standard SN model without the effects of ALPs, and $Q_{\rm heat}$ is treated as a postprocess. When $Q_{\rm heat}$ is calculated with the previous method, $Q_{\rm heat}$ increases discontinuously at $R_{\rm p} \approx 11$ km, while it rises smoothly in our method. Although the two methods are apparently different, the results for $Q_{\rm heat}$ coincide with each other at $r \gtrsim 20$ km.

[1] L. Di Luzio, M. Giannotti, E. Nardi, and L. Visinelli, Phys. Rep. **870**, 1 (2020).
[2] K. Choi, S. H. Im, and C. S. Shin, Annu. Rev. Nucl. Part. Sci. **71**, 225 (2021).
[3] G. Raffelt and L. Stodolsky, Phys. Rev. D **37**, 1237 (1988).
[4] J. Jaeckel and M. Spannowsky, Phys. Lett. B **753**, 482 (2016).
[5] M. J. Dolan, T. Ferber, C. Hearty, F. Kahlhoefer, and K. Schmidt-Hoberg, J. High Energy Phys. 12 (2017) 94.
[6] B. Döbrich, J. Jaeckel, and T. Spadaro, J. High Energy Phys. 05 (2019) 213.
[7] D. Banerjee *et al.* (NA64 Collaboration), Phys. Rev. Lett. **125**, 081801 (2020).
[8] D. Cadamuro and J. Redondo, J. Cosmol. Astropart. Phys. 02 (2012) 032.
[9] P. F. Depta, M. Hufnagel, and K. Schmidt-Hoberg, J. Cosmol. Astropart. Phys. 05 (2020) 009.
[10] P. Carenza, O. Straniero, B. Döbrich, M. Giannotti, G. Lucente, and A. Mirizzi, Phys. Lett. B **809**, 135709 (2020).
[11] M. J. Dolan, F. J. Hiskens, and R. R. Volkas, J. Cosmol. Astropart. Phys. 09 (2021) 010.
[12] J. S. Lee, arXiv:1808.10136.
[13] G. Lucente, P. Carenza, T. Fischer, M. Giannotti, and A. Mirizzi, J. Cosmol. Astropart. Phys. 12 (2020) 008.
[14] A. Sung, H. Tu, and M.-R. Wu, Phys. Rev. D **99**, 121305 (2019).
[15] A. Caputo, H.-T. Janka, G. Raffelt, and E. Vitagliano, arXiv:2201.09890.
[16] M. Giannotti, L. D. Duffy, and R. Nita, J. Cosmol. Astropart. Phys. 01 (2011) 015.
[17] J. Jaeckel, P. C. Malta, and J. Redondo, Phys. Rev. D **98**, 055032 (2018).
[18] K. Mori, Publ. Astron. Soc. Jpn. **73**, 1382 (2021).
[19] A. Caputo, P. Carenza, G. Lucente, E. Vitagliano, M. Giannotti, K. Kotake, T. Kuroda, and A. Mirizzi, Phys. Rev. Lett. **127**, 181102 (2021).
[20] A. Caputo, G. Raffelt, and E. Vitagliano, Phys. Rev. D **105**, 035022 (2022).
[21] E. O'Connor, R. Bollig, A. Burrows, S. Couch, T. Fischer, H.-T. Janka, K. Kotake, E. J. Lentz, M. Liebendörfer, O. E. B. Messer, A. Mezzacappa, T. Takiwaki, and D. Vartanyan, J. Phys. G **45**, 104001 (2018).
[22] A. Burrows and D. Vartanyan, Nature (London) **589**, 29 (2021).
[23] D. N. Schramm and J. R. Wilson, Astrophys. J. **260**, 868 (1982).
[24] T. Rembiasz, M. Obergaulinger, M. Masip, M. A. Pérez-García, M. A. Aloy, and C. Albertus, Phys. Rev. D **98**, 103010 (2018).
[25] L. di Lella, A. Pilaftsis, G. Raffelt, and K. Zioutas, Phys. Rev. D **62**, 125011 (2000).
[26] A. Kopf and G. Raffelt, Phys. Rev. D **57**, 3235 (1998).
[27] S. Reddy, M. Prakash, J. M. Lattimer, and J. A. Pons, Phys. Rev. C **59**, 2888 (1999).
[28] R. Buras, M. Rampp, H. T. Janka, and K. Kifonidis, Astron. Astrophys. **447**, 1049 (2006).
[29] T. Takiwaki, K. Kotake, and Y. Suwa, Mon. Not. R. Astron. Soc. **461**, L112 (2016).
[30] E. F. Toro, M. Spruce, and W. Speares, Shock Waves **4**, 25 (1994).
[31] J. M. Lattimer and D. F. Swesty, Nucl. Phys. **A535**, 331 (1991).
[32] M. Liebendörfer, S. C. Whitehouse, and T. Fischer, Astrophys. J. **698**, 1174 (2009).
[33] T. Takiwaki, K. Kotake, and Y. Suwa, Astrophys. J. **786**, 83 (2014).
[34] K. Kotake, T. Takiwaki, T. Fischer, K. Nakamura, and G. Martínez-Pinedo, Astrophys. J. **853**, 170 (2018).
[35] S. E. Woosley, A. Heger, and T. A. Weaver, Rev. Mod. Phys. **74**, 1015 (2002).
[36] T. Sukhbold, T. Ertl, S. E. Woosley, J. M. Brown, and H. T. Janka, Astrophys. J. **821**, 38 (2016).
[37] F. S. Kitaura, H. T. Janka, and W. Hillebrandt, Astron. Astrophys. **450**, 345 (2006).
[38] T. Yamasaki and S. Yamada, Astrophys. J. **656**, 1019 (2007).
[39] J. C. Dolence, A. Burrows, J. W. Murphy, and J. Nordhaus, Astrophys. J. **765**, 110 (2013).
[40] S. M. Couch, Astrophys. J. **775**, 35 (2013).
[41] F. Hanke, B. Müller, A. Wongwathanarat, A. Marek, and H.-T. Janka, Astrophys. J. **770**, 66 (2013).
[42] E. P. O'Connor and S. M. Couch, Astrophys. J. **865**, 81 (2018).
[43] B. Müller, T. Melson, A. Heger, and H.-T. Janka, Mon. Not. R. Astron. Soc. **472**, 491 (2017).
[44] C. D. Ott, L. F. Roberts, A. da Silva Schneider, J. M. Fedrow, R. Haas, and E. Schnetter, Astrophys. J. Lett. **855**, L3 (2018).
[45] A. Burrows, D. Radice, D. Vartanyan, H. Nagakura, M. A. Skinner, and J. C. Dolence, Mon. Not. R. Astron. Soc. **491**, 2715 (2020).
[46] R. Bollig, N. Yadav, D. Kresse, H.-T. Janka, B. Müller, and A. Heger, Astrophys. J. **915**, 28 (2021).
[47] Y. Suwa, K. Kotake, T. Takiwaki, M. Liebendörfer, and K. Sato, Astrophys. J. **738**, 165 (2011).
[48] I. Arcavi *et al.*, Astrophys. J. **721**, 777 (2010).
[49] D. Argast, M. Samland, F. K. Thielemann, and Y. Z. Qian, Astron. Astrophys. **416**, 997 (2004).
[50] T. Fischer, S. C. Whitehouse, A. Mezzacappa, F. K. Thielemann, and M. Liebendörfer, Astron. Astrophys. **517**, A80 (2010).
[51] S. Wanajo, Astrophys. J. Lett. **770**, L22 (2013).
[52] T. Fischer, N.-U. F. Bastian, M.-R. Wu, P. Baklanov, E. Sorokina, S. Blinnikov, S. Typel, T. Klähn, and D. B. Blaschke, Nat. Astron. **2**, 980 (2018).
[53] S. Zha, E. P. O'Connor, M.-c. Chu, L.-M. Lin, and S. M. Couch, Phys. Rev. Lett. **125**, 051102 (2020).
[54] T. Kuroda, T. Fischer, T. Takiwaki, and K. Kotake, Astrophys. J. **924**, 38 (2022).
[55] T. Fischer, M.-R. Wu, B. Wehmeyer, N.-U. F. Bastian, G. Martínez-Pinedo, and F.-K. Thielemann, Astrophys. J. **894**, 9 (2020).
[56] Z. G. Berezhiani, A. S. Sakharov, and M. Y. Khlopov, Sov. J. Nucl. Phys. **55**, 1063 (1992).
[57] G. Raffelt and D. Seckel, Phys. Rev. Lett. **60**, 1793 (1988).

[58] A. Burrows, M. S. Turner, and R. P. Brinkmann, Phys. Rev. D **39**, 1020 (1989).
[59] T. Fischer, S. Chakraborty, M. Giannotti, A. Mirizzi, A. Payez, and A. Ringwald, Phys. Rev. D **94**, 085012 (2016).
[60] P. Carenza, T. Fischer, M. Giannotti, G. Guo, G. Martínez-Pinedo, and A. Mirizzi, J. Cosmol. Astropart. Phys. 10 (2019) 016.
[61] T. Fischer, P. Carenza, B. Fore, M. Giannotti, A. Mirizzi, and S. Reddy, Phys. Rev. D **104**, 103012 (2021).
[62] G. Lucente and P. Carenza, Phys. Rev. D **104**, 103007 (2021).
[63] F. Calore, P. Carenza, M. Giannotti, J. Jaeckel, G. Lucente, and A. Mirizzi, Phys. Rev. D **104**, 043016 (2021).
[64] F. Calore, P. Carenza, M. Giannotti, J. Jaeckel, and A. Mirizzi, Phys. Rev. D **102**, 123005 (2020).